International Journal of Minerals, Metallurgy and Materials
Volume 28, Number 5, May 2021, Page 826
https://doi.org/10.1007/s12613-020-2223-9

In-depth analysis of the fatigue mechanism induced by inclusions for high-strength bearing steels

Chao Gu[1)], *Wen-qi Liu*[2)], *Jun-he Lian*[2)], *and Yan-ping Bao*[1)]

1) State Key Laboratory of Advanced Metallurgy, University of Science and Technology Beijing, Beijing 100083, China
2) Department of Mechanical Engineering, Aalto University, Puumiehenkuja 3, 02150 Espoo, Finland
(Received: 29 July 2020; revised: 13 November 2020; accepted: 16 November 2020)

Abstract: A numerical study of stress distribution and fatigue behavior in terms of the effect of voids adjacent to inclusions was conducted with finite element modeling simulations under different assumptions. Fatigue mechanisms were also analyzed accordingly. The results showed that the effects of inclusions on fatigue life will distinctly decrease if the mechanical properties are close to those of the steel matrix. For the inclusions, which are tightly bonded with the steel matrix, when the Young's modulus is larger than that of the steel matrix, the stress will concentrate inside the inclusion; otherwise, the stress will concentrate in the steel matrix. If voids exist on the interface between inclusions and the steel matrix, their effects on the fatigue process differ with their positions relative to the inclusions. The void on one side of an inclusion perpendicular to the fatigue loading direction will aggravate the effect of inclusions on fatigue behavior and lead to a sharp stress concentration. The void on the top of inclusion along the fatigue loading direction will accelerate the debonding between the inclusion and steel matrix.

Keywords: inclusion; high-strength bearing steel; fatigue; numerical study; stress distribution

1. Introduction

Fatigue property is one of the primary concerns of bearing steel [1–2]. With the development of advanced industry, the demand for the quality of bearing steels sharply increases. The design life and service time of bearings also increase dramatically. In certain areas, such as high-speed rail, power generation, and aerospace industry, the demand for the fatigue life of bearings exceeds 10^9 [3–6].

To meet the growing demands, researchers performed considerable works to improve the quality of bearing steel materials, including reducing impurities during smelting [7–9] and optimizing the microstructure [10–12] during rolling and heat treatment. With the ongoing efforts over centuries, the compositions and macro-defects in bearing steel can be well controlled through proper metallurgical techniques. The homogeneity of microstructure has also been significantly improved. Thereupon, the mechanical properties of bearing steel continually grow. The concepts of high-strength and ultra-high-strength steels have emerged. However, the increased strength of steel causes the increase in crack sensitivity. For the same defects or inhomogeneity in steel, such as different phases and inclusions, cracks will initiate easily in high-strength steel [13–14]. Therefore, urgent research on very high cycle fatigue (VHCF; fatigue life $>10^7$) based on high-strength steels should be conducted.

Sakai *et al.* [15–16] compared the fatigue results of the same kind of steel in rotating bending in terms of fatigue crack inducement and observed that for low cycle fatigue, the fatigue crack is usually induced by surface roughness, whereas for VHCF, fatigue cracks are usually induced by internal defects. Inclusions are the most common internal defects in steel. At the micro-level, the particularities of different inclusion features and their effects on fatigue properties, which cause large fatigue data to scatter in the VHCF regime [17], are non-negligible due to the high purity of steel. Several researchers have conducted studies on the effect of inclusions on fatigue life from the aspects of experiments and results. Karr *et al.* [18] studied the fatigue properties of steel with manganese sulfide inclusions and different densities of aluminate inclusions, reporting that the cracks initiated with different types of inclusions are related to the loading methods. Gao *et al.* [19] studied the effect of inclusions on the VHCF behavior of bainite/martensite multiphase steel with various inclusion sizes. The results showed that the fatigue crack initiated from large-sized inclusions. Spriestersbach *et al.* [20]

Corresponding author: Yan-ping Bao E-mail: baoyp@ustb.edu.cn

carried out ultrasonic fatigue tests with bainitic high-strength steel and observed that the threshold values for the stress intensity factors for VHCF are dependent on the inclusion type. These studies revealed that the features of different inclusions, including size, shape, compositions, etc., all affect the fatigue behavior in different ways. However, when analyzing the fatigue mechanism concerning inclusions, limited research focused on the interface condition between steel matrix and inclusions.

To conduct further studies on the fatigue mechanism and predict fatigue life concerning inclusions, researchers developed models at different levels to overcome the difficulty induced by the time cost of fatigue tests and the inhomogeneity of inclusion/defects distribution at the micro-level. The microstructure-based modeling study for fatigue property was initially introduced by Dunne *et al.* [21] and McDowell and Dunne [22], and further developed by Musinski and McDowell [23] and Przybyla and McDowell [24]. To study the inclusion and defects, Przybyla *et al.* [25] proposed an algorithm for estimating the cumulative probability distribution of cycles for crack formation and growth from notches with microstructure-sensitive simulation. Castelluccio and McDowell [26] exercised a microstructure-sensitive model for smooth and through-hole specimens and claimed that their three-dimensional small fatigue crack growth algorithms can quantify the most damaging loading conditions concerning strain ratios, multiaxial strain state, and mean stress. Prasannavenkatesan *et al.* [27] developed a computational strategy to characterize the driving force for fatigue crack nucleation at subsurface primary inclusions. Gillner *et al.* [28–29] adopted the representative volume element (RVE) model [30] and crystal plasticity model to predict the fatigue life of inclusion with different types. Gu *et al.* [31–32] further improved the accuracy of the RVE model by considering residual stress around inclusions. These studies continually improved the microstructure model reconstruction methods of material characteristics in three dimensions (3D) [33] and with finer resolution [34] and the accuracy of fatigue life prediction. However, experiments and simulations lacked focus on the actual interface condition between inclusions and the steel matrix. Voids and debonding may exist between inclusions and steel matrix, which will significantly affect the fatigue process. Furthermore, the cases differ for various inclusion types.

Therefore, in the present study, an in-depth experimental and numerical study on the effect of voids in the interface between different inclusions and steel matrix on the fatigue process was performed. The outcomes of the study reveal new insights into the fatigue mechanism caused by inclusions in high-strength steels under VHCF, which can provide another design variable for the development of high-strength and fatigue-resistant steels. The experimental investigation focused on the detailed analysis of the inclusion characterization and fatigue crack initiation mechanisms with qualitative and quantitative methods. To support the discovered experimental findings, using the finite element model (FEM) under different assumptions, in this work, we numerically studied the stress distribution and fatigue behavior in terms of different types of inclusions with and without voids/gaps between the inclusions and matrix. Instead of a fully quantitative prediction, the preliminary simulations results are expected to provide a consistent theoretical explanation of the new findings in terms of fatigue mechanisms.

2. Materials and experiments

The materials in this study included high-carbon bearing steel produced with different deoxidation methods: Al-deoxidation and non-Al-deoxidation. The details of the deoxidation methods and composition of the Al-deoxidation steel were described in previous research [35]. Table 1 shows the composition of non-Al-deoxidation steel. The steel billets were hot rolled into bars, vacuum quenched with oil after 20 min holding time at 835°C, and then tempered at 180°C for 120 min. Inclusions larger than 1 μm in the cross-section of the steel bars were analyzed with the inclusion auto-analysis system. The analysis area was 44.5 mm^2.

Table 1. Main composition of non-Al-deoxidation steel wt%

C	Si	Mn	P	S	Cr	Al	Total oxygen
1.000	0.246	0.322	0.0136	0.0050	1.32	0.0030	0.0011

The steels obtained after quenching and tempering were processed into hourglass-shaped specimens for fatigue tests. The specimens were acquired along the axial direction of the steel bars. Fig. 1(a) shows the geometry of the specimen conducted with an ultrasound fatigue test system under a frequency of 20 kHz. Overall, 35 specimens were involved in this study. The loading of fatigue stress in this system relied on the resonance between the amplitude magnifying horn and the specimen. The schematic diagram is shown in Fig. 1(b). During the fatigue test, air cooling was added on the fatigue specimens to protect them from overheating. The specimen temperatures were kept under 50°C. After the fatigue tests, the morphologies of the fracture surfaces were observed with scanning electronic microscopy (SEM). Crack initiation was analyzed with an energy dispersive spectrometer (EDS) to clarify the critical feature for fatigue property in the specimen. The mechanical property was also tested through tensile tests with the specimens obtained in the same direction as the fatigue specimens.

3. Modeling and simulation

The inclusion-steel matrix model was built on a micro-

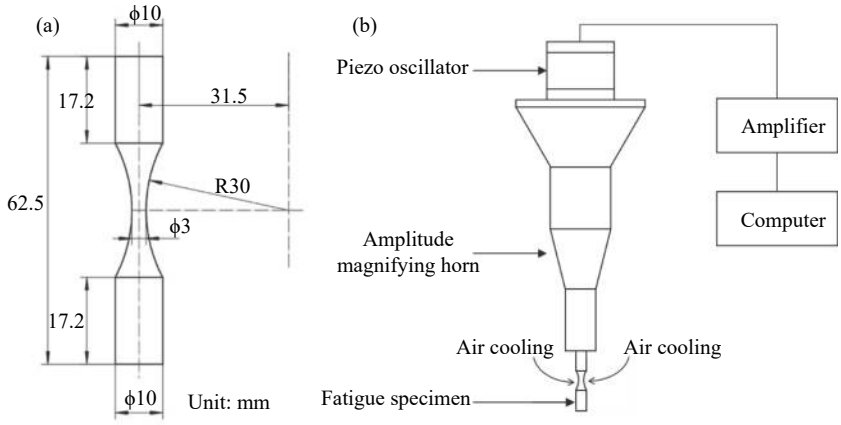

Fig. 1. Schematics of (a) the geometry of fatigue specimen and (b) the ultrasound fatigue test system.

meter scale with the commercial software Abaqus 2017 to analyze the behaviors of steel matrix and different inclusions during fatigue loading. The steel matrix was set as a 70 μm × 70 μm square with different inclusions of different shapes (spherical and quadrate) in the middle. The inclusion and steel matrix were first assumed to be tightly bonded. Afterward, a void on the interface between the inclusions and steel matrix was introduced at different places. The steel matrix was assumed to be homogeneous to highlight the stress distribution induced by inclusions during fatigue loading. Fatigue stress, which was 2200 MPa in this simulation, was selected based on the experiments. Given that the simulation particularly focused on the interface between the inclusions and matrix, and a qualitative correlation was desired, the crystal plasticity model, which can provide an in-depth interpretation of the plastic deformation with isotropic and anisotropic hardening laws of the crystal matrix [36–37], was not employed in the study. Instead, a simple isotropic Mises plasticity model formation was assumed for the steel matrix.

The boundary and interface conditions were selected carefully to avoid the inaccuracy of the simulation. In this study, the bottom side of the square steel matrix was fixed in the *x*-direction, and the left side was fixed in the *y*-direction. The square area should be a continuum in terms of mesh and deformation, enabling its collation and expansion to an infinite steel area, to guarantee the representativeness of the steel matrix. Therefore, periodic boundary conditions were also set. The element type was "continuum-plane stress-3 nodes (CPS3)". The simulation type was static.

4. Results and discussion

4.1. Mechanical properties of steel matrix

Fig. 2 shows the stress–strain curve of the high-carbon bearing steel in this study based on the results of the tensile test. The mechanical properties were obtained accordingly (Table 2).

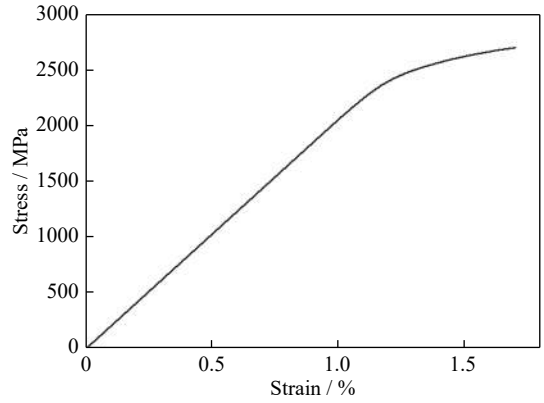

Fig. 2. Stress–strain curve of the high-carbon bearing steel used in this study.

Table 2. Mechanical properties of the high-carbon bearing steel used in this study

Yield stress / MPa	Tensile stress / MPa	Young's modulus, *E* / GPa
2502	2702	206

4.2. Inclusion characterization

Five main types of inclusions were included in the experimental bearing steels: spinel, calcium aluminate, silicate, titanium nitride, and manganese sulfide. Among these inclusions, the first four types of inclusions were all observed at the fatigue crack initiation sites. Fig. 3 shows the proportion of each inclusion in the total four types of inclusions in the virgin steel before fatigue loading and at the fatigue crack initiation sites after the tests.

As shown in Fig. 3, silicate accounted for the largest proportion among the first four types of inclusions with a narrow majority, whereas titanium nitride showed the smallest proportion. The same trend was not observed in the inclusions found at the fatigue crack initiation sites. At the fatigue crack initiation sites, the number fraction of calcium alumin-

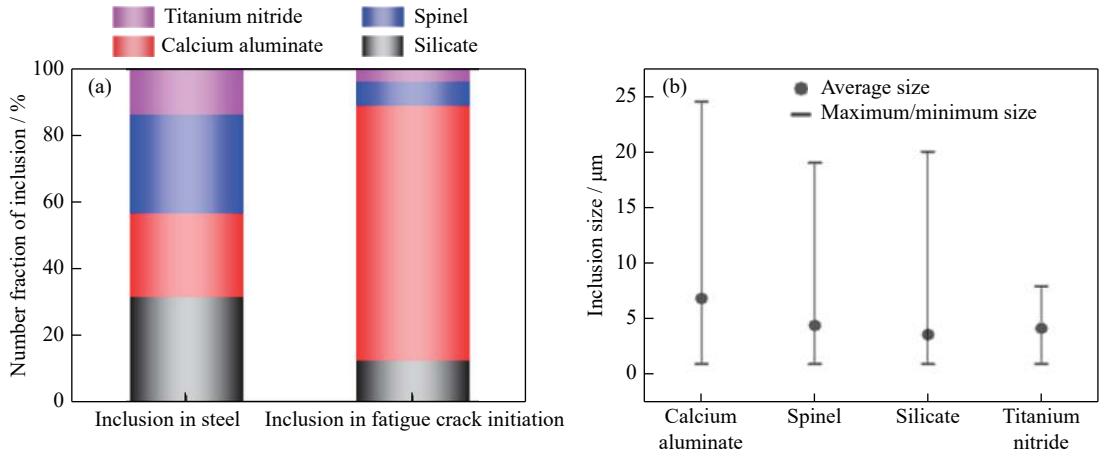

Fig. 3. (a) Comparison of inclusions in steel and at the fatigue crack initiation sites; (b) inclusion sizes.

ate inclusions was over 70%. Silicate and spinel accounted for less than 15%, although their proportion in the virgin steel before fatigue loading were over 25%.

4.3. Morphologies of fatigue fractures induced by different inclusions

After the fatigue specimens were broken, the fracture surfaces were observed by SEM. Based on the fracture morphologies, the crack initiation sites were located and analyzed with EDS. The results showed that the inclusions that triggered fatigue cracks included spinel, calcium aluminum, silicate, and titanium nitride. The characteristics of different inclusions in the crack initiation sites differed widely. Fig. 4 presents the typical appearances of the inclusions. In this study, the fatigue mechanisms caused by different inclusions were summarized to further understand fatigue stress distribution in the inclusion-steel system and provide a basis for numerical studies.

As shown in Fig. 4, the evident features of the inclusions existing at the fatigue crack initiation sites comprised i) the shape and type of inclusion, ii) presence of voids in the interface between inclusions and steels (side void/top void), and iii) cracking of the inclusion itself during the fatigue process. All these features have significant effects on stress distributions and the fatigue crack mechanism concerning inclusions. Table 3 shows a comparison of these features. According to Table 3, titanium nitride and silicate inclusions cracked during fatigue failure, whereas spinel and calcium aluminum inclusions remained unbroken and separated from one side of the specimen completely. On the interface between inclusions and steels perpendicular to the loading direction, voids surrounded the calcium aluminum inclusions, whereas spinel, silicate, and titanium nitride inclusions were tightly bonded with the steel matrix. Along the loading direction, voids also existed on the top of spinel and calcium aluminate inclusions. These voids, which enlarged during the fatigue process, may have already been generated before fatigue loading during the rolling process due to the different deformation behaviors of inclusions and steel matrix.

FEM simulations were conducted under different assumptions to further study the stress distribution and fatigue failure mechanism during the fatigue process in terms of the effect of voids adjacent to inclusions.

4.4. FEM simulation

The FEM simulation models included four types of inclusions: spinel, calcium aluminum, silicate, and titanium nitride. The mechanical properties of inclusions and steel matrix needed in this simulation were obtained from references and the results of tensile tests in the present study (Table 4). The plasticity of the steel matrix was also considered based on the result of the tensile test.

4.4.1. Stress distribution during fatigue loading when inclusions were tightly bonded with steel matrix

In the present study, the inclusions were initially assumed to be tightly bonded with the steel matrix. Fig. 5(a) shows the related geometry model. The diameter of the inclusion was 20 μm. One cycle of tension–compression was loaded on the model. Fig. 5(b) presents the loading curve. Points A and B represent the largest tension and compression, respectively.

Fig. 6 displays the stress distributions and deformations of the models in points A and B with different inclusions. The positions of maximum stress are pointed out with white arrows. The presence of inclusions led to stress concentration near the inclusions. The stress decreased gradually when the distance expanded from the inclusion. However, the largest stress and the stress distribution inside the inclusion differed distinctly in terms of various inclusion types.

As shown in Fig. 6, for the inclusions whose Young's modulus was smaller than the steel matrix, such as calcium aluminate and silicate, the stress concentrations were in the steel matrix side on the two sides of inclusions along the fatigue loading direction. Such inclusions may contribute to the generation of voids around the inclusion perpendicular to the

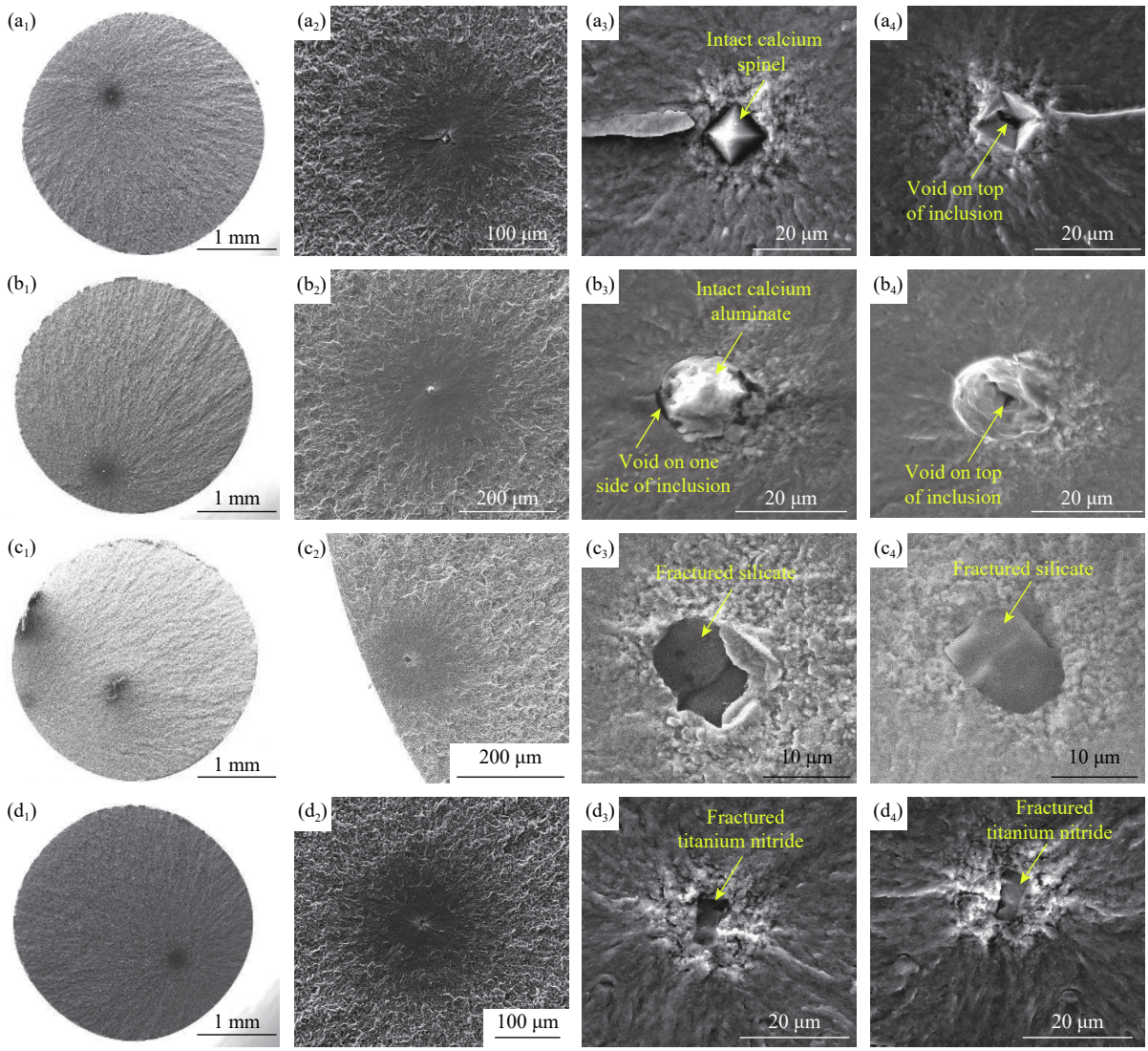

Fig. 4. Morphologies of fatigue fracture surfaces with inclusions: (a_1–a_4) spinel [35]; (b_1–b_4) calcium aluminum; (c_1–c_4) silicate; (d_1)–(d_4) titanium nitride (reproduced based on Ref. [31]).

Table 3. Comparison of different features of inclusions in fatigue crack initiations

Inclusion type	Fracture morphonology	Inclusion crack	Void on the interface between inclusions and steels	
			Side void	Top void
Spinel		×	×	√
Calcium aluminate		×	√	√
Silicate		√	×	×
Titanium nitride		√	×	×

Note: × and √ represent existence and absence of the features, respectively.

loading direction to a certain extent. During the loading process, the inclusion will give the steel matrix support against the strain caused by fatigue stress, leading to a decrease in the strain and stress concentration in the steel matrix. When the mechanical properties of the inclusions are closer to those of the steel matrix, the support will get stronger, reducing the ef-

Table 4. Mechanical properties of inclusions and steels [38–39]

Material	Young's module, E / GPa	Poisson's ratio, ν
Spinel	271	0.26
Calcium aluminum	113	0.23
Silicate	100	0.168
Titanium nitride	320	0.19
Steel	206	0.33

fect on the steel matrix during the fatigue process.

On the other hand, when Young's modulus of the inclusion is larger than that of the steel matrix, which implies a strain smaller than that of the steel matrix under fatigue loading, the stress will concentrate in the inclusion side, for example, spinel and titanium nitride. Under this circumstance, the critical fatigue condition is not generated in the steel matrix but inside the inclusion. Under an adequately large stress concentration, the inclusion (titanium nitride) will fracture before the steel matrix. The crack inside the inclusion will extend to the steel matrix during the following fatigue process. If the stress concentration is insufficient, and a debonding force exists between the inclusion and steel matrix, debonding will occur earlier than the inclusion fracture (spinel). Once the debonding begins, the gap on the interface will grow rapidly due to stress concentration on the two sides of the gap, which will be described in detail in Section 4.4.3.

4.4.2. Stress distribution during fatigue loading when voids exist around inclusions perpendicular to the loading direction

For inclusions, such as calcium aluminate, voids exist around inclusions perpendicular to the loading direction. Fig. 7(a) shows the geometry model of the inclusion-steel system. The void lies on the middle line of the square steel area. Spinel, calcium aluminum, silicate, and titanium nitride inclusions were all inserted into the model. The loading condition is the same as that in Section 4.4.1. Figs. 7(b)–7(f) show the modeling results.

As shown in Fig. 7, the void on one side of the inclusion also led to stress concentration around the void boundary, especially on the point connecting the steel, inclusion, and void. However, the maximum stress sites differed with the inclusions. For calcium aluminate, silicate, and manganese sulfide inclusions, the stress concentrated on two sides of the inclusion when voids were absent. Then the void on one side aggravated the stress concentration. Under this circumstance, the maximum stress site was located on the steel matrix adjacent to the void. For spinel and titanium nitride inclusions, stress concentrated on the inclusion without void. The existence of voids led to a region of stress concentration on the interface between the inclusion and the void, but it did not reach the peak. The maximum stress site was on the inclu-

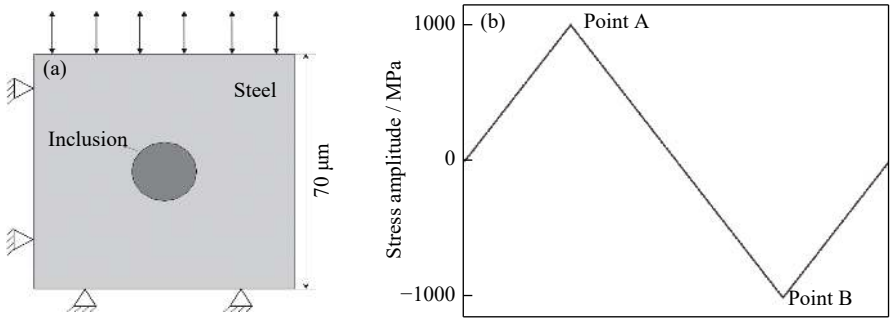

Fig. 5. (a) Geometry model of the spherical inclusion−steel system; (b) fatigue loading curve.

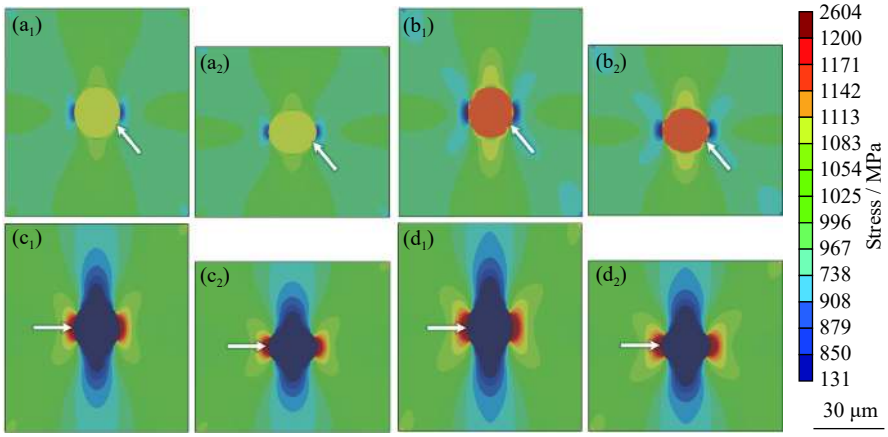

Fig. 6. Stress distributions of the models in points A and B with different spherical inclusions: (a_1, a_2) spinel; (b_1, b_2) titanium nitride; (c_1, c_2) calcium aluminum; (d_1, d_2) silicate.

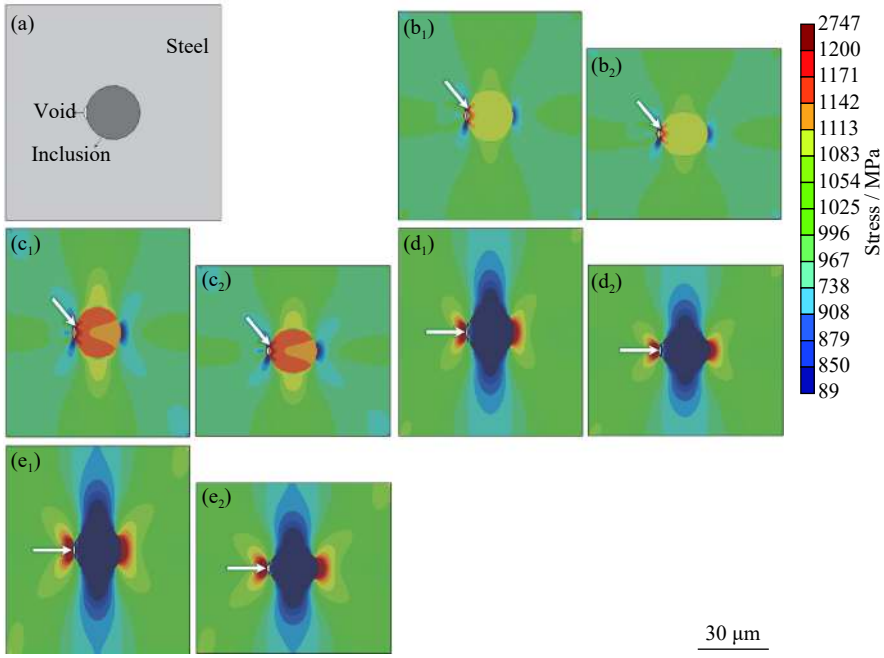

Fig. 7. (a) Geometry model of the inclusion-steel system with a void on the left side of the inclusion; stress distributions of the models in points A and B with different inclusions: (b_1, b_2) spinel, (c_1, c_2) titanium nitride, (d_1, d_2) calcium aluminum, and (e_1, e_2) silicate (white arrows point at the maximum stresses).

sion adjacent near the point connecting steel, inclusion, and void. Therefore, the void on one side of the inclusion along the loading direction will lead to crack initiation more easily than inclusions without voids. This result, may not the only reason, also solidly contribute to the fact that calcium aluminate is the most critical inclusion in bearing steels, since the calcium aluminate inclusion is the only type of inclusion with voids around the inclusion perpendicular to the loading direction.

4.4.3. Stress distribution during fatigue loading when voids are present on the top of the inclusion

Fig. 8(a) displays the geometry model of the inclusion-

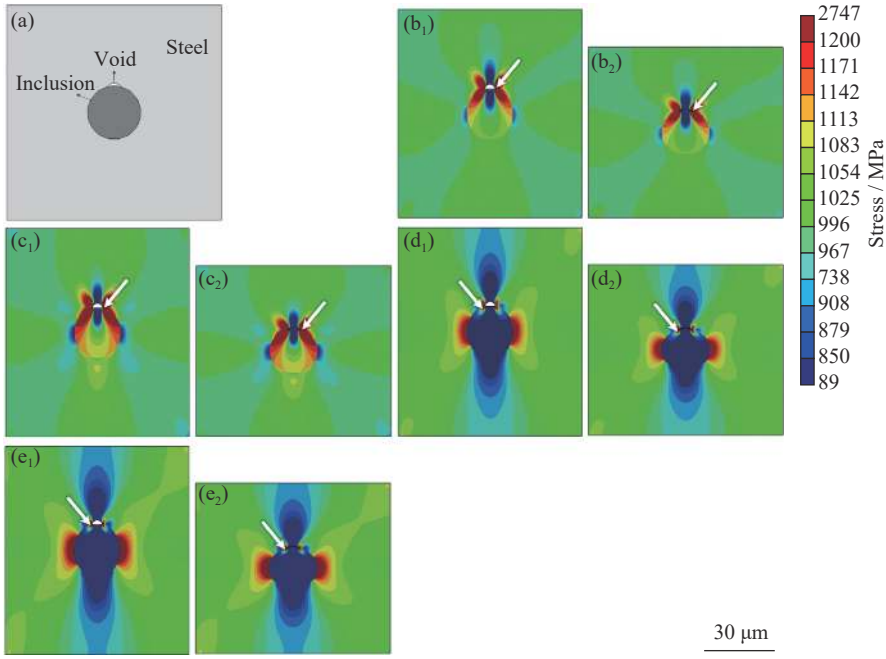

Fig. 8. (a) Geometry model of the inclusion-steel system with a void on the top of the inclusion; stress distributions of the models in points A and B with different inclusions: (b_1, b_2) spinel, (c_1, c_2) titanium nitride, (d_1, d_2) calcium aluminum, and (e_1, e_2) silicate (white arrows point at the maximum stresses).

steel system with a void on the top of the inclusion. Figs. 8(b)–8(f) show the modeling results of stress distributions with spinel, calcium aluminum, silicate, and titanium nitride inclusions.

As shown in Fig. 8, the stress concentration regions remained the same with the cases without voids. That is, when the Young's modulus of the inclusion is larger than that of the steel matrix, the stress will concentrate inside the inclusion; otherwise, the stress will concentrate in the steel matrix. In addition, in these cases, the voids in the models lead to large stress concentration and plastic strain on the two sides of the void along the loading direction, which will result in further debonding between the steel matrix and the inclusion. This further debonding also attributes to the unbroken spinel and calcium aluminate inclusions and their separation from one side of the specimen during the fatigue crack, which is consistent with the experimental results.

5. Conclusions

In the present study, stress distributions under fatigue loading in terms of the effect of voids adjacent to inclusions were numerically studied with FEM simulations. Fatigue mechanisms were also analyzed accordingly. The following conclusions can be obtained.

(1) Different inclusions exhibit various features in fatigue fracture in terms of the presence of voids on the interface between inclusions and steels (side void/top void) and cracking of the inclusion itself during the fatigue process.

(2) For the inclusions, which are tightly bonded with the steel matrix, when the Young's modulus of the inclusion is larger than that of the steel matrix (spinel and titanium nitride), the stress will concentrate inside the inclusion, leading to inclusion fracture if the stress is large enough; otherwise, the stress will concentrate in the steel matrix (calcium aluminate, silicate, and manganese sulfide), contributing to the generation of voids around inclusions perpendicular to the loading direction.

(3) The void on one side of an inclusion perpendicular to the fatigue loading direction will aggravate the effect of the inclusion on fatigue behavior and lead to a sharp stress concentration. The void on the top of inclusion alone the fatigue loading will accelerate the debonding between the inclusion and steel matrix. The top and side voids perpendicular to the loading direction exist only in the presence of calcium aluminate. This condition contributes to inclusion debonding and renders calcium aluminate as the most critical inclusion in bearing steels to a certain extent.

Acknowledgements

This work was financially supported by the Fundamental Research Funds for the Central Universities (No. FRF-TP-20-026A1), the China Postdoctoral Science Foundation (No. 2020M680348), and the State Key Laboratory of Advanced Metallurgy Foundation of China (No. 41620001).

References

[1] P. Rycerz, A. Olver, and A. Kadiric, Propagation of surface initiated rolling contact fatigue cracks in bearing steel, *Int. J. Fatigue*, 97(2017), p. 29.

[2] C. Gu, Y.P. Bao, P. Gan, M. Wang, and J.S. He, Effect of main inclusions on crack initiation in bearing steel in the very high cycle fatigue regime, *Int. J. Miner. Metall. Mater.*, 25(2018), No. 6, p. 623.

[3] N.K. Arakere, Gigacycle rolling contact fatigue of bearing steels: A review, *Int. J. Fatigue*, 93(2016), p. 238.

[4] K. Shiozawa and L. Lu, Very high-cycle fatigue behaviour of shot-peened high-carbon–chromium bearing steel, *Fatigue Fract. Eng. Mater. Struct.*, 25(2002), No. 8-9, p. 813.

[5] C. Bathias and P.C. Paris, *Gigacycle Fatigue in Mechanical Practice*, CRC Press, Boca Raton, 2004.

[6] U. Krupp, K. Koschella, and A. Giertler, The significance of grain size, segregations and inclusions for the very high cycle fatigue (VHCF) behavior of tempered martensitic steels, *Procedia Struct. Integrity*, 23(2019), p. 517.

[7] H.Y. Zheng, S.Q. Guo, M.R. Qiao, L.B. Qin, X.J. Zou, and Z.M. Ren, Study on the modification of inclusions by Ca treatment in GCr18Mo bearing steel, *Adv. Manuf.*, 7(2019), No. 4, p. 438.

[8] W.J. Ma, Y.P. Bao, M. Wang, and D.W. Zhao, Influence of slag composition on bearing steel cleanness, *Ironmaking Steelmaking*, 41(2014), No. 1, p. 26.

[9] W. Xiao, M. Wang, and Y.P. Bao, The research of low-oxygen control and oxygen behavior during RH process in silicon-deoxidization bearing steel, *Metals*, 9(2019), No. 8, art. No. 812.

[10] H.F. Xu, F. Yu, C. Wang, W.L. Zhang, J. Li, and W.Q. Cao, Comparison of microstructure and property of high chromium bearing steel with and without nitrogen addition, *J. Iron Steel Res. Int.*, 24(2017), No. 2, p. 206.

[11] Y. Xu, E.G. Wang, Z. Li, and A.Y. Deng, Effects of vertical electromagnetic stirring on grain refinement and macrosegregation control of bearing steel billet in continuous casting, *J. Iron Steel Res. Int.*, 24(2017), No. 5, p. 483.

[12] B. Shahriari, R. Vafaei, E.M. Sharifi, and K. Farmanesh, Aging behavior of a copper-bearing high-strength low-carbon steel, *Int. J. Miner. Metall. Mater.*, 25(2018), No. 4, p. 429.

[13] S.X. Li, Effects of inclusions on very high cycle fatigue properties of high strength steels, *Int. Mater. Rev.*, 57(2012), No. 2, p. 92.

[14] A. Pineau and S. Forest, Effects of inclusions on the very high cycle fatigue behaviour of steels, *Fatigue Fract. Eng. Mater. Struct.*, 40(2017), No. 11, p. 1694.

[15] T. Sakai, Y. Sato, and N. Oguma, Characteristic S–N properties of high‐carbon–chromium‐bearing steel under axial loading in long‐life fatigue, *Fatigue Fract. Eng. Mater. Struct.*, 25(2002), No. 8-9, p. 765.

[16] T. Sakai, M. Takeda, K. Shiozawa, Y. Ochi, M. Nakajima, T. Nakamura, and N. Oguma, Experimental reconfirmation of characteristic S–N property for high carbon chromium bearing steel in wide life region in rotating bending, *J. Soc. Mater. Sci. Jpn.*, 49(2000), No. 7, p. 779.

[17] H. Matsunaga, C. Sun, Y. Hong, and Y. Murakami, Dominant factors for very-high-cycle fatigue of high-strength steels and a new design method for components, *Fatigue Fract. Eng. Mater. Struct.*, 38(2015), No. 11, p. 1274.
[18] U. Karr, Y. Sandaiji, R. Tanegashima, S. Murakami, B. Schönbauer, M. Fitzka, and H. Mayer, Inclusion initiated fracture in spring steel under axial and torsion very high cycle fatigue loading at different load ratios, *Int. J. Fatigue*, 134(2020), art. No. 105525.
[19] G.H. Gao, Q.Z. Xu, H.R. Guo, X.L. Gui, B.X. Zhang, and B.Z. Bai, Effect of inclusion and microstructure on the very high cycle fatigue behaviors of high strength bainite/martensite multiphase steels, *Mater. Sci. Eng. A*, 739(2019), p. 404.
[20] D. Spriestersbach, P. Grad, and E. Kerscher, Influence of different non-metallic inclusion types on the crack initiation in high-strength steels in the VHCF regime, *Int. J. Fatigue*, 64(2014), p. 114.
[21] F.P.E. Dunne, A.J. Wilkinson, and R. Allen, Experimental and computational studies of low cycle fatigue crack nucleation in a polycrystal, *Int. J. Plast.*, 23(2007), No. 2, p. 273.
[22] D.L. McDowell and F.P.E. Dunne, Microstructure-sensitive computational modeling of fatigue crack formation, *Int. J. Fatigue*, 32(2010), No. 9, p. 1521.
[23] W.D. Musinski and D.L. McDowell, Simulating the effect of grain boundaries on microstructurally small fatigue crack growth from a focused ion beam notch through a three-dimensional array of grains, *Acta Mater.*, 112(2016), p. 20.
[24] C.P. Przybyla and D.L. McDowell, Microstructure-sensitive extreme value probabilities for high cycle fatigue of Ni-base superalloy IN100, *Int. J. Plast.*, 26(2010), No. 3, p. 372.
[25] C.P. Przybyla, W.D. Musinski, G.M. Castelluccio, and D.L. McDowell, Microstructure-sensitive HCF and VHCF simulations, *Int. J. Fatigue*, 57(2013), p. 9.
[26] G.M. Castelluccio and D.L. McDowell, Microstructure-sensitive small fatigue crack growth assessment: Effect of strain ratio, multiaxial strain state, and geometric discontinuities, *Int. J. Fatigue*, 82(2016), p. 521.
[27] R. Prasannavenkatesan, J.X. Zhang, D.L. McDowell, G.B. Olson, and H.J. Jou, 3D modeling of subsurface fatigue crack nucleation potency of primary inclusions in heat treated and shot peened martensitic gear steels, *Int. J. Fatigue*, 31(2009), No. 7, p. 1176.
[28] K. Gillner, M. Henrich, and S. Münstermann, Numerical study of inclusion parameters and their influence on fatigue lifetime, *Int. J. Fatigue*, 111(2018), p. 70.
[29] K. Gillner and S. Münstermann, Numerically predicted high cycle fatigue properties through representative volume elements of the microstructure, *Int. J. Fatigue*, 105(2017), p. 219.
[30] N. Vajragupta, P. Wechsuwanmanee, J. Lian, M. Sharaf, S. Münstermann, A. Ma, A. Hartmaier, and W. Bleck, The modeling scheme to evaluate the influence of microstructure features on microcrack formation of DP-steel: The artificial microstructure model and its application to predict the strain hardening behavior, *Comput. Mater. Sci.*, 94(2014), p. 198.
[31] C. Gu, J.H. Lian, Y.P. Bao, Q.G. Xie, and S. Münstermann, Microstructure-based fatigue modelling with residual stresses: Prediction of the fatigue life for various inclusion sizes, *Int. J. Fatigue*, 129(2019), art. No. 105158.
[32] C. Gu, J.H. Lian, Y.P. Bao, and S. Münstermann, Microstructure-based fatigue modelling with residual stresses: Prediction of the microcrack initiation around inclusions, *Mater. Sci. Eng. A*, 751(2019), p. 133.
[33] W.Q. Liu, J.H. Lian, N. Aravas, and S. Münstermann, A strategy for synthetic microstructure generation and crystal plasticity parameter calibration of fine-grain-structured dual-phase steel, *Int. J. Plast.*, 126(2020), art. No. 102614.
[34] Q.G. Xie, J.H. Lian, J.J. Sidor, F.W. Sun, X.C. Yan, C.Y. Chen, T.K. Liu, W.J. Chen, P. Yang, K. An, and Y.D. Wang, Crystallographic orientation and spatially resolved damage in a dispersion-hardened Al alloy, *Acta Mater.*, 193(2020), p. 138.
[35] C. Gu, M. Wang, Y.P. Bao, F.M. Wang, and J.H. Lian, Quantitative analysis of inclusion engineering on the fatigue property improvement of bearing steel, *Metals*, 9(2019), No. 4, p. 476.
[36] Q.G. Xie, J.H. Lian, F.W. Sun, B. Gan, and Y.D. Wang, The lattice strain ratio in characterizing the grain-to-grain interaction effect and its specific insight on the plastic deformation of polycrystalline materials, *J. Strain Anal. Eng. Des.*, 53(2018), No. 5, p. 353.
[37] Q. Xie, A.V. Bael, Y.G. An, J. Lian, and J.J. Sidor, Effects of the isotropic and anisotropic hardening within each grain on the evolution of the flow stress, the *r*-value and the deformation texture of tensile tests for AA6016 sheets, *Mater. Sci. Eng. A*, 721(2018), p. 154.
[38] D. Brooksbank and K.W. Andrews, Tessellated stresses associated with some inclusions in steel, *J. Iron Steel Inst.*, 207(1969), p. 474.
[39] D. Brooksbank and K.W. Andrews, Thermal expansion of some inclusions found in steels and relation to tessellated stresses, *J. Iron Steel Inst.*, 206(1968), p. 595.